

Full paper

“Water-in-deep eutectic solvent” electrolytes enable zinc metal anodes for rechargeable aqueous batteries

Jingwen Zhao^a, Jian Zhang^b, Wuhai Yang^c, Bingbing Chen^a, Zhiming Zhao^{a,d}, Huayu Qiu^e, Shanmu Dong^a, Xinhong Zhou^e, Guanglei Cui^{a,*}, Liquan Chen^f

^a Qingdao Industrial Energy Storage Research Institute, Qingdao Institute of Bioenergy and Bioprocess Technology, Chinese Academy of Sciences, Qingdao 266101, China

^b College of Chemistry and Chemical Engineering, Qingdao University, Qingdao 266071, China

^c School of Polymer Science and Engineering, Qingdao University of Science and Technology, Qingdao 266042, China

^d University of Chinese Academy of Sciences, Beijing 100049, China

^e College of Chemistry and Molecular Engineering, Qingdao University of Science and Technology, Qingdao 266042, China

^f Beijing National Laboratory for Condensed Matter Physics, Institute of Physics, Chinese Academy of Sciences, Beijing 100190, China

ARTICLE INFO

Keywords:

Zn anodes
Deep eutectic solvents
Low cost batteries
Aqueous electrolytes
Water molecules

ABSTRACT

Metallic zinc (Zn) is one of the most promising anodes for aqueous batteries, but so far its applicability for rechargeable systems remains elusive, mainly owing to the free water-induced parasitic reactions. Here, we report a new “water-in-deep eutectic solvent (water-in-DES)” electrolyte (~30 mol.% H₂O in a eutectic mixture of urea/LiTFSI/Zn(TFSI)₂; TFSI, bis(trifluoromethanesulfonyl)imide), in which all water molecules participate in DES's internal interaction (H-bonding and coordinating) network, leading to a suppressed reactivity with Zn anode from both thermodynamic and electrochemical aspects. Inheriting characteristics from aqueous and DES media, this electrolyte enables stable and reversible Zn plating/stripping with over twentyfold enhancement in cycling life compared to routine aqueous electrolytes, even at low rates. With these merits, a desirable rechargeability (> 90% capacity retention after 300 cycles at 0.1 C) is achieved for a 1.92 V (average discharge voltage) Zn/LiMn₂O₄ battery, together with a practical energy density of 52 Wh/kg (pouch cell, 2 Ah, ~9.8 × excess Zn on anode).

1. Introduction

Zn metal battery (ZMB) family has a rich history as an important area in the electrochemical power supply [1–5]. Primary ZMBs (e.g., Zn/MnO₂, Zn/Ag and Zn/air batteries) are still commercially viable [6–10]. Although lithium-ion batteries (LIBs) with high efficiency and energy density currently dominate energy-storage landscape, their implementation at large scale faces a huge challenge because of the limited lithium availability, high cost and safety risk [11–13]. Hence, the century-old ZMBs have been revisited and made rechargeable in recent years, in view of the huge global reserves of Zn and the innate safety arising from applying aqueous electrolytes [14–17]. Different from traditional ZMBs, several ion-storage materials are now chosen as cathodes to couple with Zn anodes for improving energy outputs [18–24]. Among these, the Zn/LiMn₂O₄ (Zn/LMO) cell is particularly favorable because of its high voltage (1.8–2.0 V) and ameliorative interfacial ion transfer behavior [25–27]. Even with this renewed effort, the main obstacle that has yet to be overcome lies in the poor

reversibility of aqueous Zn chemistry [6,28,29]. A deep understanding of the interfacial compatibility between Zn metal and electrolyte is imperative, especially at the development stage.

It is known that aqueous electrolytes are able to support the Zn²⁺ → Zn⁰ process (the electroplating technology) and the Zn⁰ → Zn²⁺ process (the primary ZMBs), respectively. As for the rechargeable function, however, the required thermodynamic and electrochemical stabilities of Zn metal have been difficult to achieve in the routine metal salt-containing aqueous environment [3]. The main reason is that free water, as the dominant component, participates in all the parasitic reactions [4,30]. Specifically, unlike organic electrolyte systems that can form a solid-state interphase by sacrificial electrolyte decomposition at the initial charging states, a competing H₂ evolution reaction (HER) inevitably occurs in aqueous electrolytes during each recharging cycle due to the low Zn/Zn²⁺ potential (−0.76 V vs. NHE) [2,31,32]. Such irreversible process builds up internal pressure and induces Zn pulverization, eventually leading to cell failure even in trace amounts of H₂ (Fig. 1a). Some temporary methods, like adopting mild acidic

* Corresponding author.

E-mail address: cuiql@qibebt.ac.cn (G. Cui).

<https://doi.org/10.1016/j.nanoen.2018.12.086>

Received 15 October 2018; Received in revised form 16 December 2018; Accepted 28 December 2018

Available online 29 December 2018

2211-2855/ © 2018 Elsevier Ltd. All rights reserved.

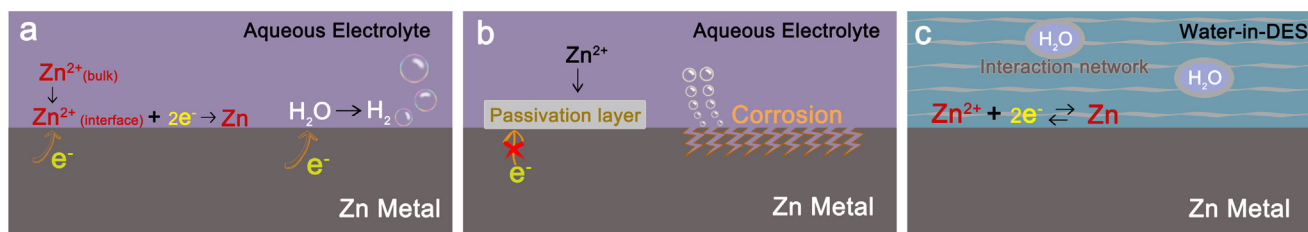


Fig. 1. (a,b) Schematic diagrams of interfacial reactions on Zn anode in the presence of traditional aqueous electrolytes: (a) the Zn plating process accompanied by the electrochemical H₂ evolution, and (b) passivation and corrosion due to the thermodynamic instability. (c) Reversible Zn electrochemistry in the water-in-DES electrolyte.

electrolyte or relatively high cycling rate can restrain this negative effect, but non-faradaic reactions, namely corrosion and passivation [30,33–35] have to be also emphasized (Fig. 1b). These detrimental processes also facilitate the electrolyte depletion, reduce the utilization of Zn, and thus cause the short shelf/cycling life.

Actually, many strategies have been proposed over past decades, such as adding electrolyte additives, alloying and constructing hierarchical structures, to alter the electrochemical behavior of Zn anodes [5,36–40]. Despite this progress, it remains a dilemma for the aqueous electrolyte design to realize a side reaction-free Zn deposition. Deep eutectic solvents (DESs), generally obtained by simply mixing Lewis acids and bases in the eutectic molar ratio, have emerged as attractive alternatives to ionic liquids [41,42]. Due to the high degree of design freedom, many types of metal salt-containing DESs were proposed and applied to electroplating [43–46] and electropolishing [47,48]. Notably, coordinating and H-bonding species (ions or molecules) within DESs make them strongly water-miscible and highly hygroscopic. Although absorbed water significantly affects the physicochemical properties of DESs, there is an upper limit to this hydration, below which DES's nature can be retained and water molecules tend to be isolated from each other [49–52]. This favorable trend could be leveraged for exploring new aqueous electrolyte systems with tailored adaptability toward Zn anode.

In the present work, we present that a stable and effective aqueous electrolyte, which involves incorporating controlled amounts of water (~6 wt%, ~30 mol.%) into a urea-based DES matrix, endows Zn anode with unusual reversibility and durability (Fig. 1c). A combination of the spectroscopic analysis and theoretical modelling reveals that the intensified water-DES interactions significantly suppress the water reactivity while the merits of aqueous system on the ionic conductivity and viscosity are inherited. Along with the retaining eutectic feature, this “water-in-DES” electrolyte brings a stable cycling property with high capacity retention (> 80% after 600 cycles at 0.5 C, > 90% after 300 cycles at 0.1 C) for high-voltage Zn/LMO batteries. The reliability on long-term cycling has been further ascertained by pouch-cell (2 Ah) assembly and testing.

2. Experimental

2.1. Electrolyte preparation

The pristine DES samples (defined as LZ-DES) were formed by mixing the three components (LiTFSI, Zn(TFSI)₂ and urea; TFSI, bis(trifluoromethanesulfonyl)imide) with the required molar ratios (the LiTFSI/urea molar ratio between 1:3 and 1:3.8, and the LiTFSI/Zn(TFSI)₂ M ratio kept at 20) in an argon-filled glove box (Table S1). Clear and colorless liquids can be obtained directly after heating the mixtures at around 90 °C overnight with gentle stirring. These LZ-DES samples were further purged under vacuum for 24 h at a temperature of 60 °C. The water-in-DES electrolytes (defined as LZ-DES/*n*H₂O; *n* refers to the H₂O/Li molar ratio; *n* ≤ 2; Table S2) were prepared by adding ultrapure water (> 18.0 MΩ) to the above LZ-DES samples, followed by shaking and standing for approximately 24 h at room temperature.

Subsequently, the electrolytes were stored in an inert atmosphere for further use. The samples of L-DES and L-DES/*n*H₂O were prepared by a similar procedure, except for the absence of Zn(TFSI)₂.

2.2. Material characterizations

The morphology of the samples was characterized by a field emission scanning electron microscope (SEM, Hitachi S-4800). X-ray diffraction (XRD) patterns were recorded in a Bruker-AXS Micro-diffractometer (D8 ADVANCE) with Cu-Kα1 radiation ($\lambda = 1.5405 \text{ \AA}$). The fluorescence and optical images of the samples were obtained using a BX51 Fluorescence Microscope (Olympus). Raman spectra were recorded at room temperature using a Thermo Scientific DXRXI system with excitation from an Ar laser at 532 nm. A differential scanning calorimeter (TA, dsc250) is used to evaluate the thermal properties of the electrolytes. Samples are scanned from -80 – 40 °C at a rate of 5 °C min⁻¹ under a nitrogen atmosphere. Fourier transform infrared spectroscopy (FTIR) measurements were carried out on a Perkin-Elmer spectrometer in the transmittance mode. An attenuated total reflectance (ATR) attachment with a diamond crystal was used to obtain IR spectra. A small volume of the electrolyte solutions (less than 5 μ L) was needed to cover the surface of the diamond crystal. During measurements, an alumina lid was utilized to isolate samples from the atmosphere, so as to minimize the influence of moisture. The ¹⁷O NMR analyses were conducted with a Bruker AV400 spectrometer (25 ± 0.1 °C), using 5 mm tubes.

2.3. Differential electrochemical mass spectrometry tests

The differential electrochemical mass spectrometry (DEMS) experiments were done with an ECC-Air cell (EL-CELL GmbH, Germany). The in situ cell was equipped with a gas inlet and outlet (Fig. S3) and connected to an HPR-20 QIC Benchtop Gas mass spectrometer with a backing and bypass scroll pump. The electrochemical measurements were tested with a LAND CT2001A system. During the electrochemical measurements, a constant stream of argon (flow rate of 0.5 mL/min) can take any gas products from the DEMS cell to the mass spectrometer. Electrodes (Zn foil and LMO) and separators were 18 mm in diameter.

2.4. Fabrication of coin cells and pouch cells

Cathode electrodes comprised LMO (80 wt%) or LiFePO₄ (LFP, 80 wt%), Super P carbon (10 wt%), and polyvinylidene fluoride (10 wt %). Slurries containing these components in N-methyl-2-pyrrolidone were cast onto stainless steel (SS) foils (5 μ m in thickness) by the doctor blading method. The active mass loading for cathode materials was ~ 5.0 mg/cm² for coin cells and ~ 9.6 mg/cm² for pouch cells (both sides of SS foils). Coin cells were assembled in open atmosphere by sandwiching a glass fiber paper soaked with electrolyte between the prepared cathode electrodes and Zn foils (~ 13.6 mg/cm²). The pouch-type ZMBs (2 Ah) were further assembled by the multilayered stacking configuration with the cellulose nonwoven membrane (50 μ m in thickness) as the separator.

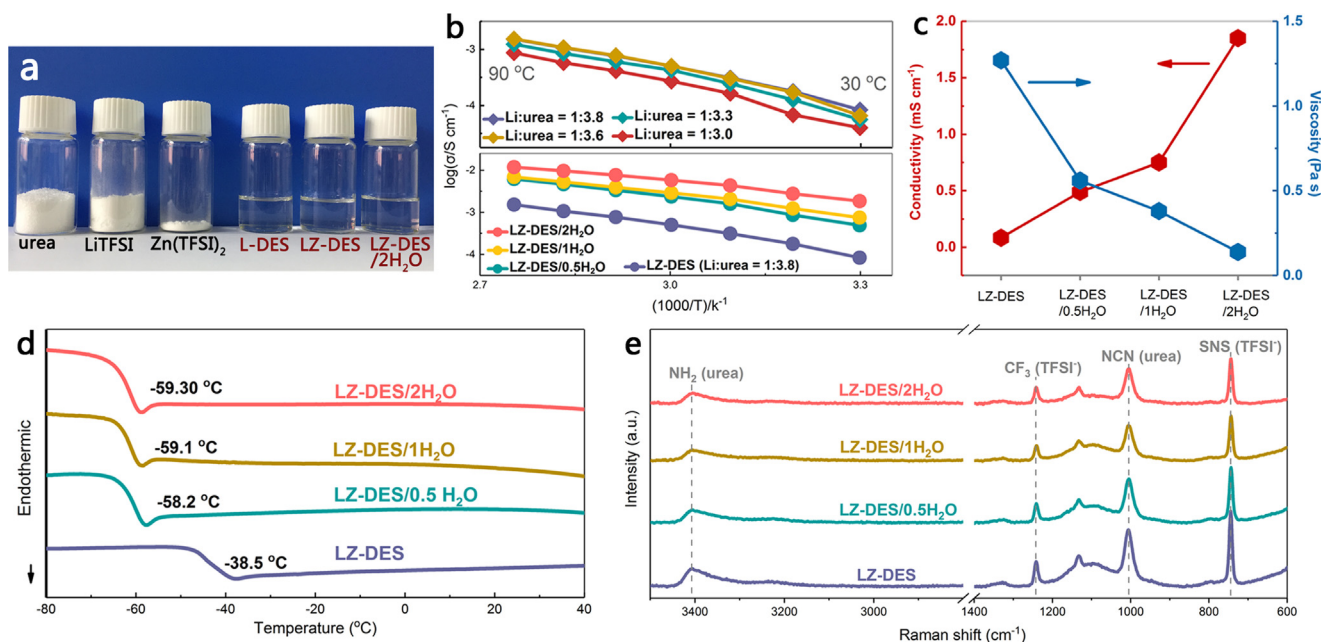


Fig. 2. Preparation and characterization of the water-in-DES solutions. (a) Stoichiometric amounts of urea, LiTFSI and Zn(TFSI)₂ used to prepare L-DES, LZ-DES and LZ-DES/2H₂O. (b) Temperature-dependent ionic conductivity for (top) LZ-DES with various Li/urea ratios and (bottom) LZ-DES/nH₂O with different water contents. (c) Variation of viscosity and conductivity for the LZ-DES/nH₂O solutions with increasing the water content (30 °C). (d) DSC and (e) Raman results for the LZ-DES/nH₂O and the pristine LZ-DES (the Li/urea ratio of 1:3.8).

3. Results and discussion

To demonstrate the availability of our strategy, a DES system containing two active ions (Li⁺ and Zn²⁺), denoted as LZ-DES, was first prepared, in which urea, LiTFSI and Zn(TFSI)₂ served as main components. TFSI⁻ was chosen as the anion because of its plasticizing effect and weak Lewis basicity [53,54]. These LZ-DESs are liquid at ambient temperatures and remain stable without any heat treatment when components were mixed in an appropriate molar ratio range (the Li/urea molar ratio between 1:3 and 1:3.8, and the Li/Zn molar ratio kept at 20; Fig. 2a and Table S1). Note that the eutectic system without Zn(TFSI)₂ (L-DES) is also the liquid state. The Li/urea ratio of 1:3.8 gives LZ-DES the highest conductivity of 0.084 mS/cm at 30 °C (Fig. 2b). After the addition of small amounts of water, homogenous and clear solutions (described as LZ-DES/nH₂O; molar ratio: $n = \text{H}_2\text{O}/\text{Li} = 0.5, 1$ and 2; Table S2) were further obtained with significantly reduced viscosity (0.139 Pa s for LZ-DES/2H₂O at 30 °C) and enhanced conductivity (1.85 mS/cm for LZ-DES/2H₂O at 30 °C; Fig. 2b–c). This LZ-DES/nH₂O system is much lower in terms of the vapour pressure (1.04 kPa for LZ-DES/2H₂O at 30 °C) than the common aqueous solutions (4.25 kPa for pure water at 30 °C), which deviates from Raoult's law [55]. This observation presents a thermodynamically decreased water activity in a manner somewhat analogous to the hydrate-melt electrolytes [54].

Differential scanning calorimetry (DSC) measurement detected an approximately 20 °C decrease in the freezing points for LZ-DES/nH₂O as compared to LZ-DES (Fig. 2d). This is naturally related to the increase in degree of disorder (lower entropic difference of phase transition) and consequent sluggish crystallization for eutectic mixtures [51,56]; namely, water molecules are more likely to participate in forming stronger bonds with DES components rather than appearing as a separate phase. For the pristine LZ-DES, the interplay among the components is clearly indicated by obvious changes throughout the Raman spectra (Fig. S1). Upon closer examination, the introduction of water only induces a negligible redshift in characteristic bands of urea and TFSI⁻ (Fig. 2e), demonstrating that the eutectic nature of LZ-DES remains intact under the conditions of relatively low water contents.

Thus, the water-in-DES definition can reasonably apply to these solutions, as the water state and chemical environment (i.e., solvating ions, H-bonding) are significantly altered from those in diluted aqueous electrolytes (shown later). After comprehensive considerations of physicochemical properties, the LZ-DES/2H₂O with Li/urea ratio of 1:3.8 was chosen as the electrolyte to investigate its potential application in ZMBs unless otherwise noted.

Zn anode is widely used in primary aqueous batteries but has hardly functioned reversibly because of the intensive parasitic reactions during recharging [57]. For an overall understanding, the chemical stability of Zn in different electrolytes was first investigated (Fig. 3a). As comparison, after immersion in the typical aqueous electrolytes (0.25 M Li₂SO₄ + 0.5 M ZnSO₄ and 0.5 M LiTFSI + 0.5 M Zn(TFSI)₂) for 15 days, Zn foils tarnished and formed complex coatings, apparently associated with the non-faradaic reactions. In LZ-DES/2H₂O, however, no visible change was observed. Fig. 3b–j summarizes the results of post-mortem Zn surface morphology characterization by a combination of fluorescence microscope, optical microscope and SEM. It is evident from the figure that the most remarkable difference was observed when the comparison aqueous electrolytes were used, where micron-scale passive aggregates were accumulated on Zn (corresponding XRD results are shown in Fig. S2). This unstable interface behavior restricts conventional aqueous electrolytes available to rechargeable ZMB applications despite their various advantages.

In situ analysis of electrolyte compatibility with Zn was conducted by differential electrochemical mass spectrometry (DEMS), known as one of the most effective techniques to detect gas evolution. It is worth noting that the weak acidity of dilute aqueous electrolytes leads to spontaneous chemical H₂ evolution once being in contact with metallic Zn. This issue can be directly reflected in the open-circuit voltage (OCV) step of a Zn||Zn cell assembled by 0.5 M LiTFSI + 0.5 M Zn(TFSI)₂ (Fig. 3k and S3). When current pulses of 0.05 and 0.1 mA/cm² were applied, the electrochemically induced H₂ peaks appeared along with the ionic current track from OCV process. As for LZ-DES/2H₂O, no H₂ evolution was observed during the entire operando testing. Such a difference is more discernible from in situ optical microscopy of Zn deposition in a home-made cell (Fig. S4), and the time-lapse images are

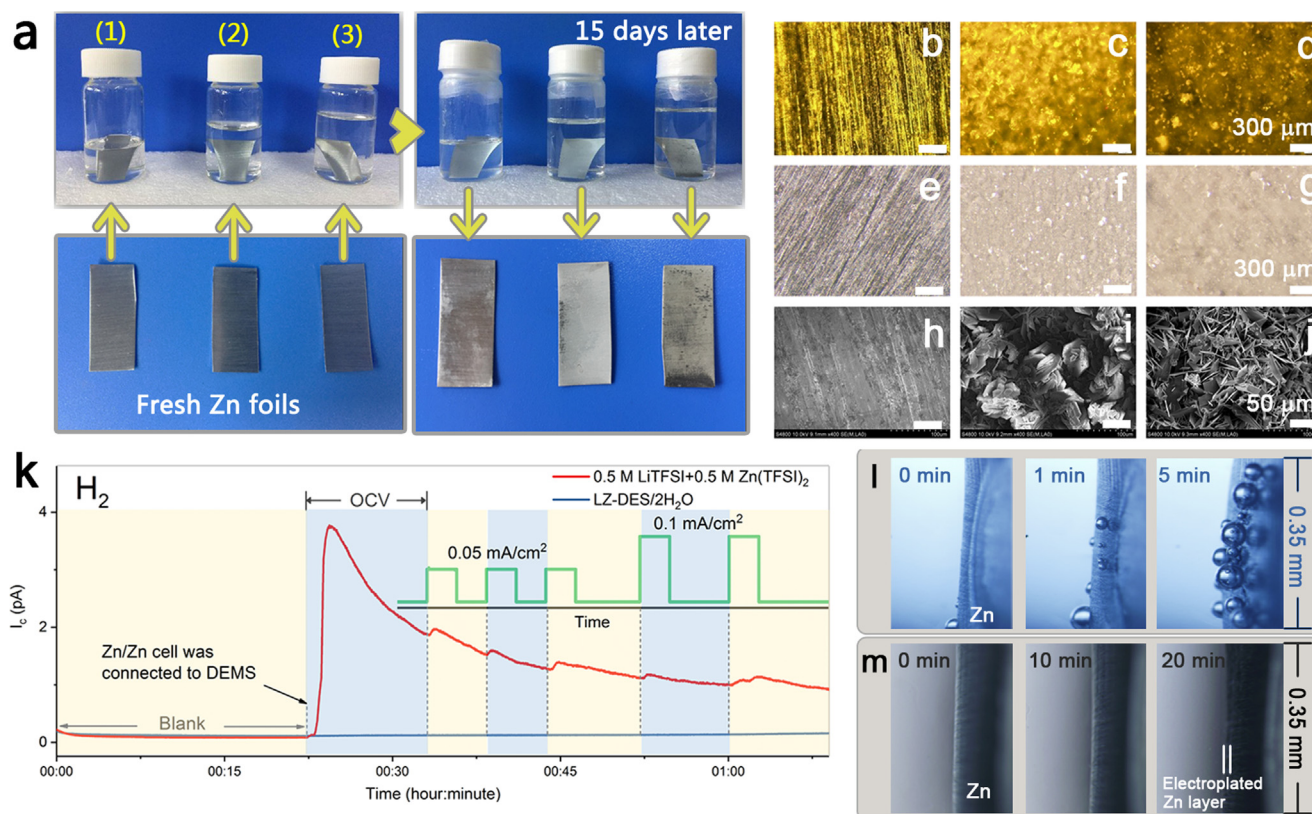


Fig. 3. Chemical and electrochemical compatibilities of aqueous electrolytes with Zn metal. (a) Reactivity of Zn foils with (1) LZ-DES/2H₂O, (2) 0.25 M Li₂SO₄ + 0.5 M ZnSO₄ and (3) 0.5 M LiTFSI + 0.5 M Zn(TFSI)₂ at room temperature (left: initial state; right: 15 days later). The surface morphology of Zn foils after immersion in (b,e,h) LZ-DES/2H₂O, (c,f,i) 0.25 M Li₂SO₄ + 0.5 M ZnSO₄ and (d,g,j) 0.5 M LiTFSI + 0.5 M Zn(TFSI)₂ using a combination of (b–d) fluorescence microscope, (e–g) optical microscope and (h–j) SEM. (k) Online DEMS data for Zn||Zn cells with 0.5 M LiTFSI + 0.5 M Zn(TFSI)₂ and LZ-DES/2H₂O, respectively (inset: the profile of applied current densities). Before being connected to the DEMS, the cells experienced a prolonged standing of 20 mins to check the chemical H₂ evolution. Then, the currents of 0.05 and 0.10 mA/cm² were applied to monitor the electrochemical H₂ evolution. In situ optical microscopic images of the Zn electrodeposition process in (l) 0.5 M LiTFSI + 0.5 M Zn(TFSI)₂ and (m) LZ-DES/2H₂O at 0.2 mA/cm².

shown in Fig. 3l–m. The dilute aqueous electrolyte suffers from gas (i.e., H₂) bubbling, significantly interrupting Zn deposition. In contrast, a dendrite-free Zn layer was achieved for cell using LZ-DES/2H₂O after 40 mins at 0.2 mA/cm². This situation can be also detected by naked eyes in the case of Zn deposition onto Ti (Fig. S5). Hence, both chemical and electrochemical stabilities of Zn are significantly increased in the present water-in-DES electrolyte.

Further galvanostatic plating/stripping measurements were carried out to investigate the effects of electrolytes on reversible Zn deposition. Fig. 4a exhibits the results of cycling experiments in Zn||Zn cells at a rate of 0.1 mA/cm². In stark contrast to the sudden voltage fluctuation in 0.5 M LiTFSI + 0.5 M Zn(TFSI)₂ after ca. 120 h, the cell with LZ-DES/2H₂O initially experienced an induction period of 30 h, and then cycled steadily over 2400 h (3.3 months) without pronounced overpotential build-up. Stable cycling performance is also observed using a pure LZ-DES electrolyte, despite a slight amplified polarization (Fig. S6). Noted that the reversibility of metallic anodes also depends on the charge-discharge rate; side reactions at the electrolyte/electrode interface are believed to be more competitive at relatively low rates [13,58]. Thus, the voltage evolution was further examined at a low rate of 0.02 mA/cm² with the charge/discharge interval being extended to 10 h (Fig. 4b). It is apparent from figure that traditional aqueous electrolytes are quite sensitive to the rate, and their cells exhibit premature failures, in as little as 20 h of operation (i.e., first cycle), which is consistent with the unstable interface and the resulting hindrance of Zn²⁺ transport. Surprisingly, for LZ-DES/2H₂O, the Zn plating/stripping cycling remains remarkably stable even after 400 h, with symmetrical voltage response observed in each cycle. This nearly twentyfold enhancement

in cycling life achieved by the water-in-DES electrolyte underscores its suitability in rechargeable ZMB applications. Post-mortem SEM analysis indicates that the electrolyte of 0.5 M LiTFSI + 0.5 M Zn(TFSI)₂ forms thick, loose dendritic structures/by-products on Zn while LZ-DES/2H₂O provides a finer and more compact surface (Fig. S7a–b). Furthermore, the marked difference in the interfacial charge-transfer behavior upon cycling in Zn||Zn cells can be verified by the electrochemical impedance spectroscopy (EIS; Fig. S7c–f).

Given the fact that Zn source is limited in full cells, Coulombic efficiency (CE) is significant for evaluating how long the metallic anode would survive. CEs in these electrolytes were measured in Zn||SS cells at a practical deposition capacity of 0.5 mAh/cm² and a current density of 0.5 mA/cm² (Fig. 4c–f). The erratic stripping signals seen in cells based on the routine aqueous electrolytes can be undoubtedly attributed to the water decomposition and resulting competitive gas evolution [13]. LZ-DES/2H₂O shows a smooth and regular voltage profile as well as much higher CEs (96.2%, 11th cycle) compared to those of routine aqueous electrolytes (< 50%, 11th cycle). This factor can be further optimized by choosing other substrates (for example, Au, Cu or Ti). Besides, the relatively high overpotential of Zn plating/stripping in water-in-DES electrolyte could be alleviated by reducing its viscosity using non-aqueous additives or tailoring the DES composition [46,51].

The electrochemical window (EW) of water-in-DES electrolytes was evaluated in a three-electrode cell with a SS foil as working electrode (Fig. 4g). In a typical aqueous electrolyte (0.5 M LiTFSI), the hydrogen and oxygen evolution reactions (HER and OER) are clearly indicated by two irreversible processes, one cathodic below 0 V and one anodic above 2.2 V, respectively. Because the operation potentials of Zn and

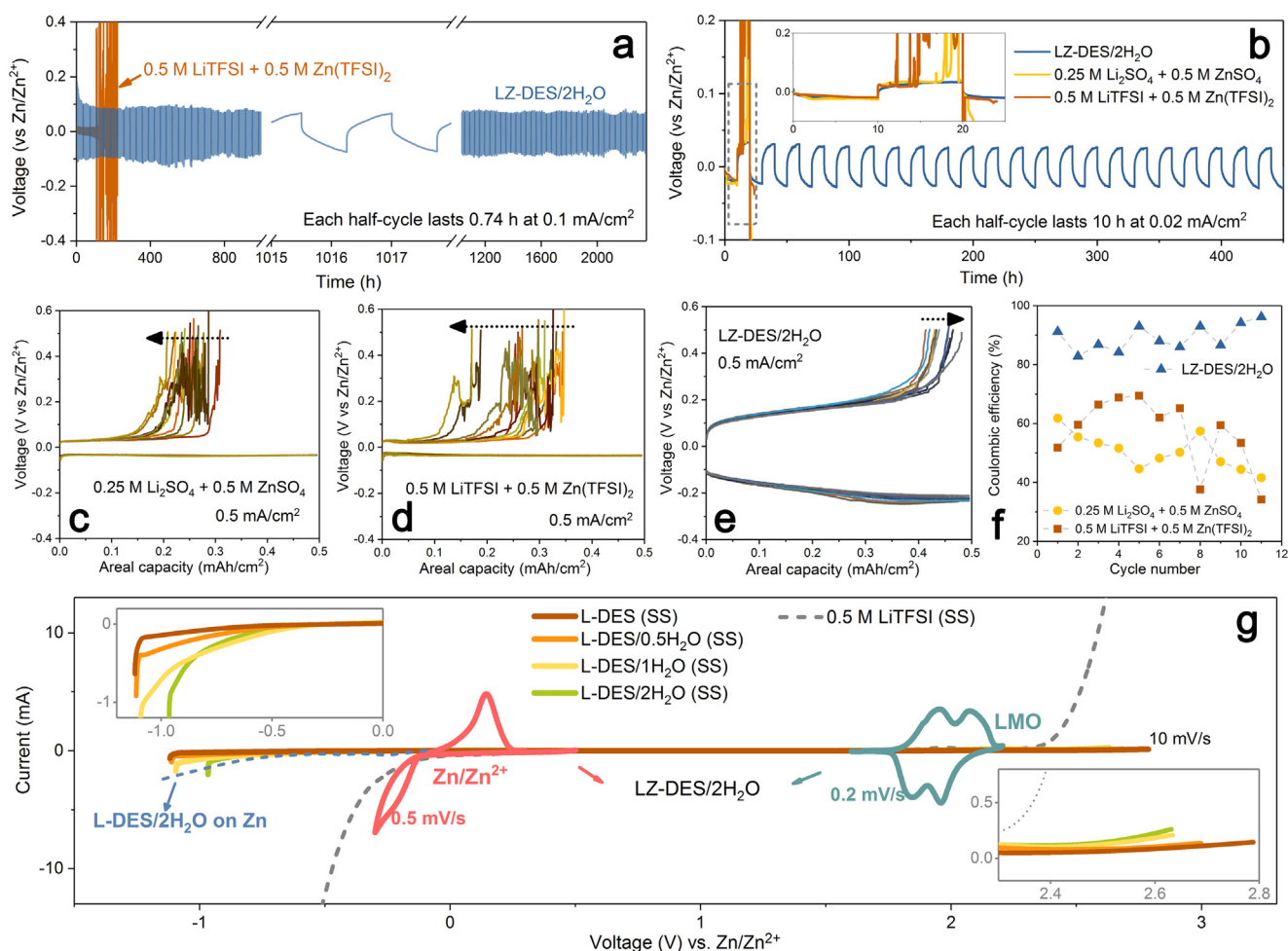


Fig. 4. Electrochemical reversibility and stability of Zn anodes in different electrolytes. (a) Voltage profiles in a Zn||Zn symmetrical cell at 0.1 mA/cm² (each half cycle lasting for 0.74 h). (b) Voltage profiles in a Zn||Zn symmetrical cell at 0.02 mA/cm² (each half cycle lasting for 10 h). The inset in (b) is zoomed-in segment of the first cycle. The cells made with dilute aqueous electrolytes show a sudden polarization and then fail during the first cycle, whereas the LZ-DES/2H₂O-based cell performs prolonged cycles with an over 20-fold improvement. (c–e) Voltage profiles and (f) Coulombic efficiency (CE) of Zn plating/stripping using a Zn||stainless steel (SS) cell (0.5 mA/cm²). (g) The electrochemical stability window of the pristine LZ-DES and LZ-DES/*n*H₂O electrolytes on the non-active SS (insets are the enlarged views on cathodic and anodic sides) and cyclic voltammograms (CVs) of Zn/Zn²⁺ deposition/stripping processes (SS as the working electrode) and LMO (coated on SS) in LZ-DES/2H₂O. The blue dashed line represents the cathodic potential window of LZ-DES/2H₂O on Zn.

LMO locate near these stability limits [20], the active materials unfortunately exhibit low CEs as well as obvious capacity fading (Fig. S8 and S9). By contrast, the LZ-DES/*n*H₂O electrolytes exhibit significantly expanded EWs (> 2.5 V), affording valid coupling of Zn and LMO. LMO has been considered to be one of the most promising cathode materials for aqueous batteries due to its high redox potential and structural stability. With the LZ-DES/2H₂O electrolyte, the two pairs of redox peaks shown in the range between 1.85 and 2.2 V (cyan CV curve in Fig. 4g) are consistent with the typical two-phase lithiation/de-lithiation inherent to LMO [20,29]. No other processes, like co-intercalation of Zn²⁺ and electrolyte decomposition, were detected (Fig. S21). More importantly, the extension for the cathodic limit can be also obtained on the metallic Zn substrate (blue dashed line in Fig. 4g). Despite a slight narrowing of EW with adding water in pristine LZ-DES (insets in Fig. 4g), both HER and OER are pushed well beyond the thermodynamic stability limits of routine aqueous electrolytes, validating DEMS results (Fig. 3k). Moreover, as either a dilute or an additive, water is beneficial in reducing the viscosity and consequently, in refining metallic species diffusion, as demonstrated by the reduced polarization (Fig. 4a and S6) and increased current response upon Zn/Zn²⁺ reactions (Fig. S10). For practical applications, a balance between the reduction in EW and the enhancement in electrochemical kinetics must be maintained by regulating the water content and identifying the

specific water state in the DES.

FTIR was applied for monitoring the molecular state of water. For bulk liquid water, the typical broad band of stretching modes located at 3000–3800 cm⁻¹ has been found to be sensitive to the environment and intermolecular interactions. Although the stretching bands of urea unavoidably interfere with refined analyses in this area (Fig. 5a), a distinct band at ~3600 cm⁻¹ appears with the addition of water and becomes increasingly obvious for the water content up to 6.18 wt% (LZ-DES/2H₂O). The new band is characteristic of chemically bonded water (the ν_{as} mode) [59–61], in sharp contrast to the observations from common aqueous solutions. This finding suggests that adding reasonable amounts of water in LZ-DES does not lead to aggregates or pools of free water, but the isolated water molecules possibly interacting with DES components, in line with the depressed freezing points in DSC results (Fig. 2d). No obvious change was found for the bands of urea and TFSI⁻ (Fig. S11), further verifying the eutectic network is largely retained. However, with further increasing the water content, the bands from 3100 to 3500 cm⁻¹ and around 1640 cm⁻¹ gradually broaden, indicative of the presence of free water clusters (Fig. S12). Thus, the water-in-DES definition is only suitable for present LZ-DES/*n*H₂O electrolytes with water contents below 6.18 wt% (*n* ≤ 2).

The water state was further determined by ¹⁷O NMR spectroscopy, as shown in Fig. 5b. For a 0.5 M LiTFSI control with free water being the

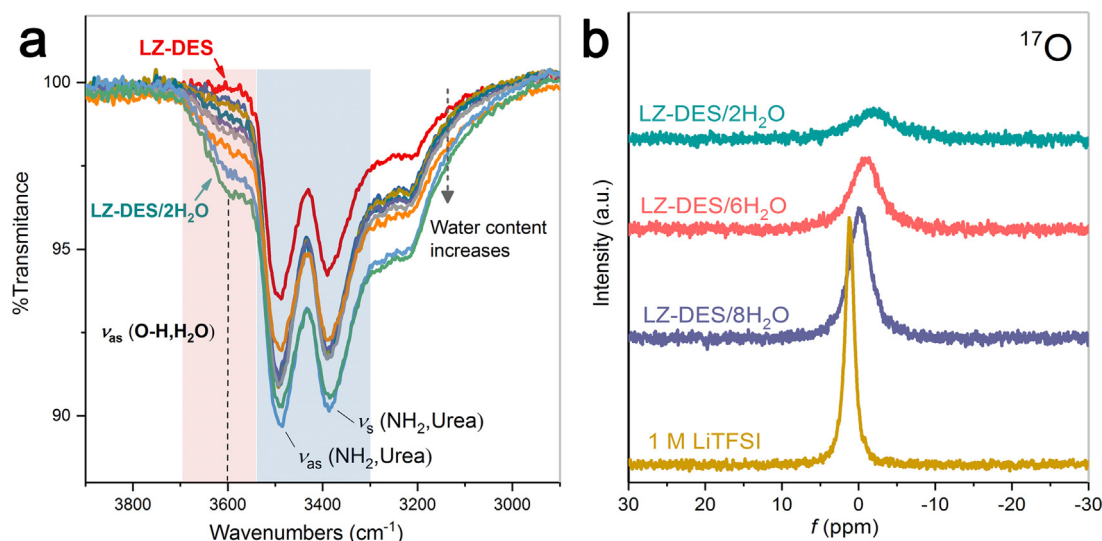


Fig. 5. Spectrum analysis of water state. (a) Progression of IR bands observed in the range of $2900\text{--}3900\text{ cm}^{-1}$ with increasing water content in LZ-DES. (b) The chemical shifts for ^{17}O nuclei (water) in LZ-DES/ $n\text{H}_2\text{O}$ and 0.5 M LiTFSI .

dominant species, a distinct water ^{17}O resonance was clearly detected around 0 ppm . However, this signal shifts to lower frequency (i.e., upfield) as the LZ-DES content increases. This remarkable change is ascribed to a gradual transition from free water to bound water and the resulting varied charge distribution on water oxygen [29,61]. In other words, the introduction of DES likely breaks the water-water H-bonded network, and simultaneously traps the water molecules by intensified O–H (water)–DES and H–O (water)–DES interactions.

To theoretically elucidate the electrolyte structure, density functional theory based molecular dynamics (DFT-MD) simulations were performed. All the equilibration structures were obtained at 300 K . For the water-free L-DES (molar ratio: urea/LiTFSI = 18:5), a highly ordered interaction network can be found (Fig. S13): each Li^+ is coordinated by four or three carbonyl oxygen atoms from urea while all TFSI $^-$ anions are hydrogen bonded to urea. This theoretical structure of the eutectic liquid is in agreement with the observation from the Raman spectra (Fig. S1). As water is introduced (molar ratio: LiTFSI/ H_2O = 1:1 and 1:2), this network is slightly reorganized. It is clear from Fig. 6a–d that all water molecules are confined in the DES matrix via H-bonding with urea and TFSI $^-$ (cyan dashed lines), and intruding into the Li^+ -coordination structure. Meanwhile, no free water molecules were detected in both L-DES/ H_2O and L-DES/ $2\text{H}_2\text{O}$. The resulting radial distribution functions (rdfs; also called pair correlation functions) between different molecules/ions describes probability distributions of nearest-neighbor molecules at a certain distance, as displayed in Fig. 6e–f. Despite of anticipated weakening of the DES-DES interactions (urea-TFSI and Li-urea) by water [41,50,52], the electrolyte system retains most of the eutectic essence. This unique electrolyte structure supports the spectroscopy results described in Fig. 5 and rationalizes the suppression of free water-induced parasitic reactions on Zn anode as discussed above. Nevertheless, the present water-in-DES system is clearly distinct from pure DES, since water contributes to the new bonding structures and introduces features of aqueous system. Further analysis of H_2O -Li, H_2O -urea and H_2O -TFSI rdfs demonstrates the water's preference for interplaying with metal cations over other species (Fig. S14). This feature may be beneficial to the interfacial charge transfer [25,26] and also accounts for the decreased polarization of Zn/ Zn^{2+} reactions [62–65].

The available potential ranges of electrolytes were compared in a Zn/LMO cell by a galvanostatic method (Fig. 7a). For the electrolyte of $0.5\text{ M LiTFSI} + 0.5\text{ M Zn(TFSI)}_2$, the charging limits are shown to be 1.91 V , 1.95 V and 2.00 V at 0.06 C , 0.12 C and 0.3 C (based on the mass of LMO), respectively. As expected, LZ-DES/ $2\text{H}_2\text{O}$ increases the

available voltage limit positively by $> 0.3\text{ V}$ at each rate. It is known that parasitic reactions could be kinetically hidden at high rates, causing an overestimated reversibility [58]. Thus, a low rate would more accurately reflect what electrolytes perform in an actual ZMB. Below 0.2 C , the water decomposition observed in $0.5\text{ M LiTFSI} + 0.5\text{ M Zn(TFSI)}_2$ dramatically interrupts the LMO redox reactions, as exhibited by in situ observation by DEMS (Fig. S15). As for LZ-DES/ $2\text{H}_2\text{O}$, typical plateaus related to the LMO de-lithiation with highly suppressed gas production are starkly visible at all applied rates. DEMS further lends support to this electrochemical reliability (Fig. S16).

The compatibility of LZ-DES/ $2\text{H}_2\text{O}$ with both cathode and anode has been witnessed by voltage profiles of ZMB (Fig. 7b). At 0.06 C , the cell delivers a discharge capacity of 117 mAh/g , based on the mass of the LMO only. The profile in the initial cycle slightly differs from the followed ones, corresponding to the gradual activation of the electrodes and the electrode-electrolyte interfaces. Upon closer comparison with the redox plateaus in different electrolytes (Fig. 7a–b), an apparent positive shift of $\sim 0.11\text{ V}$ occurred at the cell utilizing LZ-DES/ $2\text{H}_2\text{O}$, which produces an unprecedented average discharge voltage of 1.92 V , substantially higher than those in traditional aqueous electrolytes [11,66,67]. The redox behaviors of LMO in different electrolytes were analyzed by using a Ag/AgCl reference electrode (Fig. 7c). Compared with those in $0.5\text{ M LiTFSI} + 0.5\text{ M Zn(TFSI)}_2$, two cathodic peaks of LMO show a positive shift by $\sim 0.10\text{ V}$ in LZ-DES/ $2\text{H}_2\text{O}$. This value is close to the change of the operation voltage range for Zn/LMO cell between dilute aqueous and water-in-DES electrolytes. For faradic Li^+ -insertion electrode materials, the modulation of redox processes towards positive potentials caused by the Li^+ activity change (according to the Nernst equation) has been observed in previous works on highly concentrated electrolytes [54,68]. Due to the synchronous upward shifts on both cathode and anode, the voltages of resulting full cells with single active ion (Li^+) remain unchanged. Nevertheless, the present LZ-DES/ $2\text{H}_2\text{O}$ electrolyte contains a much higher concentration of Li^+ compared with that of Zn^{2+} (molar ratio of $\text{Li}/\text{Zn} = 20$), and these two ions support their respective redox processes without interference from each other, which leads to a distinct difference in potential shift between Zn and LMO (Fig. 7d). More direct evidence was obtained from the charge-discharge comparison by using a Zn/LFP analogue (Fig. S17), in which LZ-DES/ $2\text{H}_2\text{O}$ indeed realizes a 0.12 V increase in operating voltage. This nonsynchronous modulation is unique for hybrid ion-based battery chemistries, and also offers a promising strategy for engineering high-voltage energy storage devices.

Thanks to the high voltage output, an energy density of 224.6 Wh/

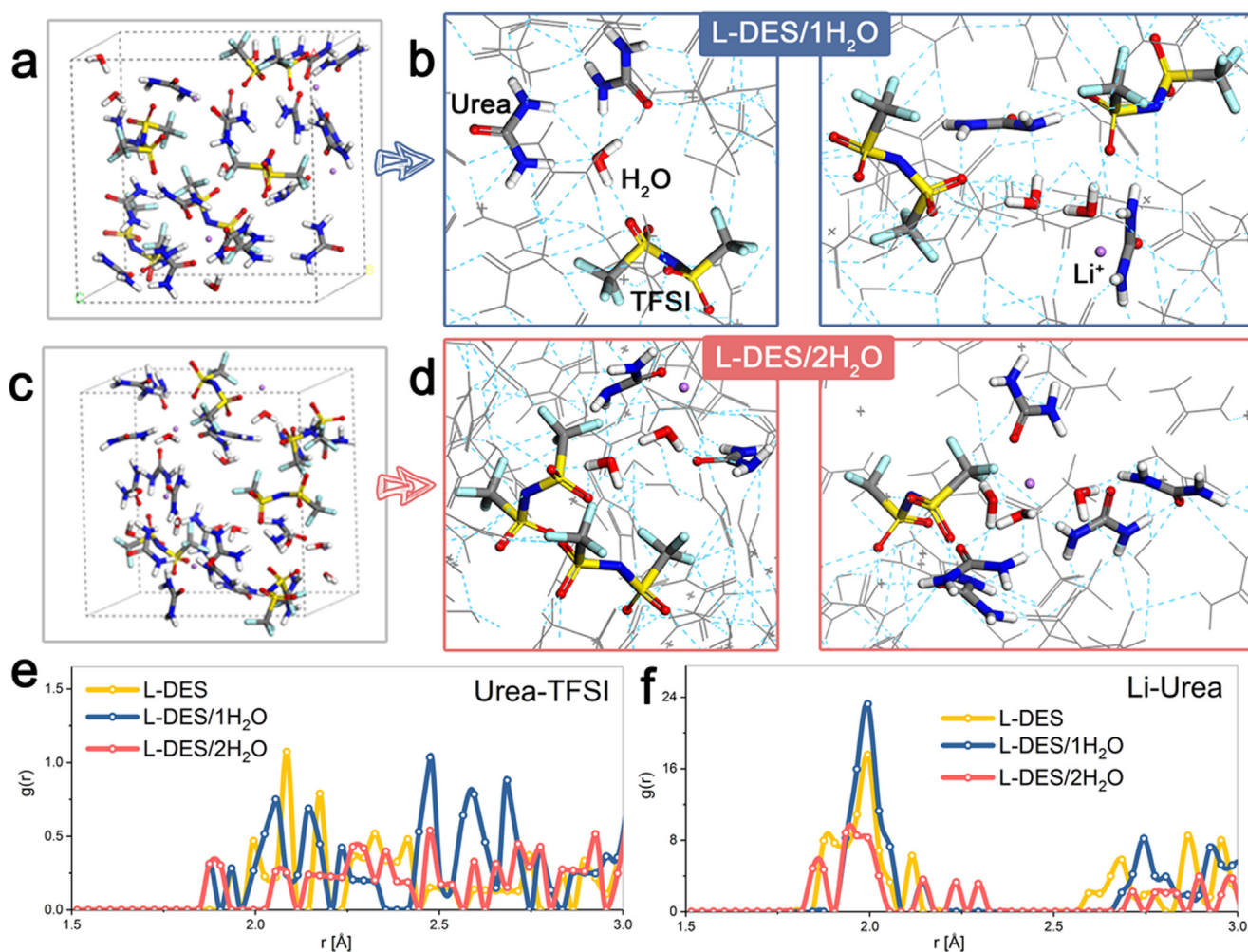


Fig. 6. Theoretical analysis of the water-in-DES electrolyte. (a–d) Snapshots of equilibrated electrolyte systems and representative interaction structures of H₂O molecules (H-bonding with urea and TFSI⁻, and coordination with Li⁺) for (a,b) L-DES/1H₂O and (c,d) L-DES/2H₂O (Li, purple; N, blue; O, red; C, gray; S, yellow; F, light green; H, white; cyan dashed lines represent the H-bonding) obtained by DFT-MD simulations. All-atom rdfs for (e) urea-TFSI and (f) Li-urea in L-DES, L-DES/1H₂O and L-DES/2H₂O at 298 K and 1 bar.

kg is achieved based on LMO. The cell capacity only decreases by 30% when the rate increases from 0.06 C to 1.0 C (Fig. S18). After over 30 cycles upon continuously varied rates, a considerable capacity of 114 mAh/g is still maintained, indicating a desirable rate performance supported by LZ-DES/2H₂O. Fig. 7e compares cycling performance of Zn/LMO cells with various electrolytes, and corresponding CEs are shown in Fig. 7f. Not surprisingly, abnormal charge-discharge response, inefficient charge process and huge capacity loss signify the limitation of routine aqueous electrolytes for rechargeable ZMBs (Fig. S19–S20). As for LZ-DES/2H₂O, much higher CEs and lower capacity fading rate are achieved; for example, 90.8% (after 300 cycles), 82.7% (after 600 cycles) and 86.6% (after 600 cycles) of the discharge capacities have been retained at 0.1 C, 0.5 C and 2 C, respectively. Corresponding morphology change of LMO cathode after cycling is shown in Fig. S21a–b. Note that the pure LZ-DES can also act as an electrolyte for ZMBs (Fig. S22–S24). However, due to its relatively high viscosity, the polarization of Zn/LMO and Zn/LFP cells was amplified and capacities slightly decreased.

Aside from the laboratory-scale coin cells, we also assembled pouch-type ZMBs with a capacity of 2000 mAh to further demonstrate the efficacy of our water-in-DES electrolyte (Fig. 8d). It has to be noted that a truly ideal ZMB should employ just bare current collector (0 × excess of Zn) at the beginning. However, to maintain the contact surface area and balance the electric field, thin Zn foils (13.6 mg/cm², 11.2 mAh/

cm², ~9.8 × excess) were still used with the sacrifice of a large part of energy density. Besides, the estimation of energy density has to take the electrolyte into account if in a practical manner. Contrary to the typical “rocking-chair” mechanism in LIBs, all the active Zn on the anode comes from the pristine electrolyte for the present Zn/LMO system [67]. Thus, the full-cell energy density is overly dependent on the electrolyte weight and the Zn salt solubility. To alleviate this limitation, the partially delithiated Li_xMn₂O₄ (x ≈ 0.5) was applied for the pouch-type ZMBs.

Of note, owing to the insensitivity of water-in-DES electrolytes to moisture and air, the present ZMB system does not require expensive and strictly controlled assembly procedures and environment, as do LIBs. As shown in Fig. 8a–b, the pouch cell with LZ-DES/2H₂O maintains an average CE of > 96.0% and exhibits an 84.8% capacity retention after 160 cycles, which are commercially acceptable. On the basis of the total weight of the present pouch cell, an energy density of 52 Wh/kg has been achieved (with room for improvement by optimizing the initial Zn inventory on the anode and by coupling with other high-voltage cathode materials), which is comparable to Ni–MH (60–120 Wh/kg) and higher than lead–acid (25–50 Wh/kg) batteries [69,70]. Post-mortem SEM analysis demonstrates a dendrite-free surface morphology of Zn anode after cycling (Fig. 8c). By contrast, in the case of the aqueous electrolyte of 0.5 M LiTFSI + 0.5 M Zn(TFSI)₂, the pouch cell suffers from serious capacity decay arising from detrimental

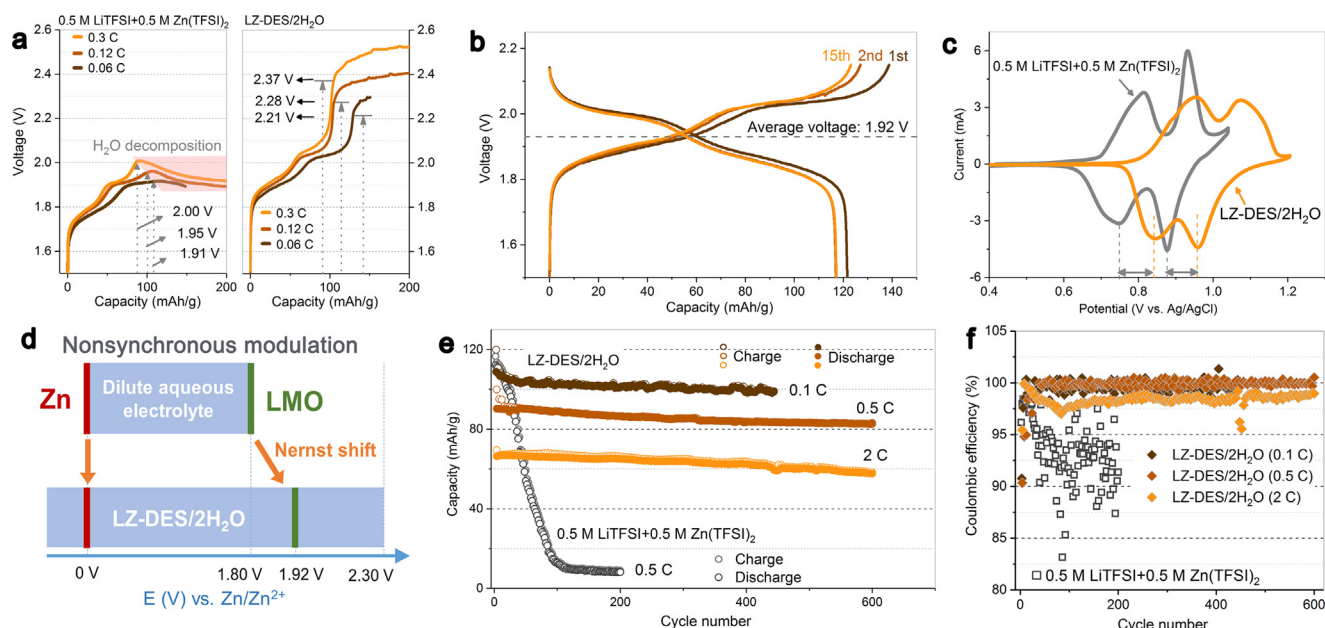


Fig. 7. Electrochemical performance of ZMBs. (a) The available charging limits of Zn/LMO cells with different electrolytes. (b) Charge-discharge profiles (0.06 C based on LMO) of Zn/LMO cell in LZ-DES/2H₂O. (c) CVs of LMO in different electrolytes. (d) The relation between the potential windows (blue bands) and redox reaction potentials of Zn (red lines) and LMO (green lines) in dilute aqueous electrolyte and LZ-DES/2H₂O. The redox reaction potential of LMO is shifted upward while that of Zn remains steady according to the Nernst equation (blue regions represent the electrochemical stability windows). (e) Cycling performance and (f) CE of the Zn/LMO cell in LZ-DES/2H₂O under various rates, in comparison with those in 0.5 M LiTFSI + 0.5 M Zn(TFSI)₂.

parasitic reactions, as demonstrated by the formation of complex products on the Zn anode (Fig. 8e) and the drastic expansion of the cell (Fig. 8f).

4. Conclusions

Extensive research on rechargeable ZMBs has re-emerged recently; however, the poor compatibility of aqueous electrolytes with Zn metal remains a huge challenge. Based on the online characterization, we uncovered that passivation, corrosion and water decomposition

inevitably occur on Zn anode in the presence of mild aqueous electrolytes, as exemplified by 0.5 M LiTFSI + 0.5 M Zn(TFSI)₂ and 0.25 M Li₂SO₄ + 0.5 M ZnSO₄. To overcome this issue, we developed a new water-in-DES electrolyte system by simply regulating the water/DES ratio, in which the water reactivity maintains a remarkably depressed level due to the formation of well-defined eutectic network. Featured with the characteristics (low viscosity and high conductivity, etc.) from aqueous media and the better stability from DES, this electrolyte is able to make the Zn anode chemically robust and electrochemically reversible, which produces a superior rechargeability for ZMBs

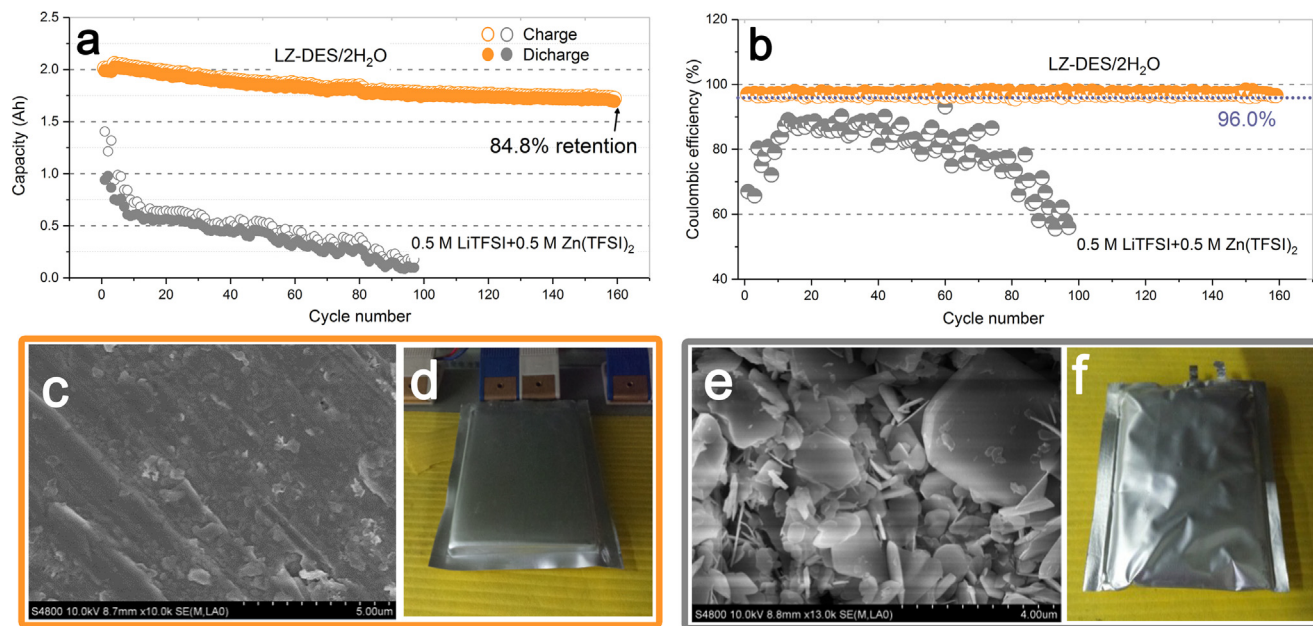


Fig. 8. High-capacity pouch-type ZMBs. (a) Galvanostatic cycling performance and (b) corresponding CE of Zn/LMO pouch cells (with 9.8 × excess Zn) using LZ-DES/2H₂O (between 1.5 V and 2.15 V) and 0.5 M LiTFSI + 0.5 M Zn(TFSI)₂ (between 1.5 V and 1.95 V) at room temperature and 0.2 C. Post-mortem SEM analysis of Zn anodes and digital pictures of pouch cells using (c,d) LZ-DES/2H₂O and (e,f) 0.5 M LiTFSI + 0.5 M Zn(TFSI)₂ after cycling.

A nonsynchronous Nernst modulation of redox processes, unique for the hybrid battery chemistry, has been also explored, which realizes a ~0.11 V upward shift in the operating voltage for Zn/LMO cells. Moreover, based on the water-in-DES electrolyte, a 2 Ah pouch-type cell was demonstrated to achieve an energy density of 52 Wh/kg (based on the total device mass) and a long lifespan with acceptable capacity retention (84.8% after 150 cycles). We believe that this strategy of engineering an internal structure of eutectic system brings about a promising way to address the intrinsic problems of Zn anodes and pouches rechargeable ZMBs into the realm of practical applications.

Acknowledgement

This work was supported by the Programs of the National Natural Science Foundation of China (Grant No. 21601195, 51625204, 21671196), Qingdao Science and Technology Program (17-1-1-30-jch), Key Scientific and Technological Innovation Project of Shandong (Grant No. 2017CXZC0505) and Qingdao Key Lab of Solar Energy Utilization & Energy Storage Technology. G. C. particularly appreciates the financial aid from the China National Funds for Distinguished Young Scientists of the National Natural Science Foundation of China. The authors gratefully acknowledge Prof. Andrew P. Abbott for helpful discussions.

Appendix A. Supplementary material

Supplementary data associated with this article can be found in the online version at doi:10.1016/j.nanoen.2018.12.086.

References

- [1] X.-P. Gao, H.-X. Yang, *Energy Environ. Sci.* 3 (2010) 174–189.
- [2] H. Kim, G. Jeong, Y.-U. Kim, J.-H. Kim, C.-M. Park, H.-J. Sohn, *Chem. Soc. Rev.* 42 (2013) 9011–9034.
- [3] D. Linden, T.B. Reddy, *Handbook of Batteries*, 3rd ed., McGraw-Hill, 2002.
- [4] F.R. McLarnon, E.J. Cairns, *J. Electrochem. Soc.* 138 (1991) 645–656.
- [5] J.F. Parker, C.N. Chervin, I.R. Pala, M. Machler, M.F. Burz, J.W. Long, D.R. Rolison, *Science* 356 (2017) 415–418.
- [6] R. Dell, *Solid State Ion.* 134 (2000) 139–158.
- [7] Z. Liu, T. Cui, G. Pullettikurthi, A. Lahiri, T. Carstens, M. Olschewski, F. Endres, *Angew. Chem. Int. Ed.* 55 (2016) 2889–2893.
- [8] T.J. Simons, D.R. MacFarlane, M. Forsyth, P.C. Howlett, *ChemElectroChem* 1 (2014) 1688–1697.
- [9] A. Stani, W. Taucher-Mautner, K. Kordesch, J. Daniel-Ivad, Development of flat plate rechargeable alkaline manganese dioxide–zinc cells, *J. Power Sources* 153 (2006) 405–412.
- [10] J. Vatsalarani, N. Kalaiselvi, R. Karthikeyan, *Ionics* 15 (2009) 97–105.
- [11] Z. Chang, Y. Yang, M. Li, X. Wang, Y. Wu, *J. Mater. Chem. A* 2 (2014) 10739–10755.
- [12] X. Liang, Q. Pang, I.R. Kochetkov, M.S. Sempere, H. Huang, X. Sun, L.F. Nazar, *Nat. Energy* 2 (2017) 17119.
- [13] L. Suo, O. Borodin, Y. Wang, X. Rong, W. Sun, X. Fan, S. Xu, M.A. Schroeder, A.V. Cresce, F. Wang, *Adv. Energy Mater.* (2017) 1701189.
- [14] D. Kundu, B.D. Adams, V. Duffort, S.H. Vajargah, L.F. Nazar, *Nat. Energy* 1 (2016) 16119.
- [15] H. Li, C. Han, Y. Huang, Y. Huang, M. Zhu, Z. Pei, Q. Xue, Z. Wang, Z. Liu, Z. Tang, *Energy Environ. Sci.* 11 (2018) 941–951.
- [16] A.R. Mainar, L.C. Colmenares, J.A. Blázquez, I. Urdampilleta, *Inter. J. Energy Res.* 42 (2018) 903–918.
- [17] P. Senguttuvan, S.D. Han, S. Kim, A.L. Lipson, S. Tepavcevic, T.T. Fister, I.D. Bloom, A.K. Burrell, C.S. Johnson, *Adv. Energy Mater.* 6 (2016) 1600826.
- [18] T. Gupta, A. Kim, S. Phadke, S. Biswas, T. Luong, B.J. Hertzberg, M. Chamoun, K. Evans-Lutterodt, D.A. Steingart, *J. Power Sources* 305 (2016) 22–29.
- [19] G. Li, Z. Yang, Y. Jiang, C. Jin, W. Huang, X. Ding, Y. Huang, *Nano Energy* 25 (2016) 211–217.
- [20] J. Yan, J. Wang, H. Liu, Z. Bakonov, D. Gosselink, P. Chen, *J. Power Sources* 216 (2012) 222–226.
- [21] P. Hu, M. Yan, T. Zhu, X. Wang, X. Wei, J. Li, L. Zhou, Z. Li, L. Chen, L. Mai, *ACS Appl. Mater. Interfaces* 9 (2017) 42717–42722.
- [22] F. Wan, L. Zhang, X. Dai, X. Wang, Z. Niu, J. Chen, *Nat. Commun.* 9 (2018) 1656–1656.
- [23] N. Zhang, F. Cheng, Y. Liu, Q. Zhao, K. Lei, C. Chen, X. Liu, J. Chen, *J. Am. Chem. Soc.* 138 (2016) 12894–12901.
- [24] P. Hu, T. Zhu, X. Wang, X. Wei, M. Yan, J. Li, W. Luo, W. Yang, W. Zhang, L. Zhou, Z. Zhou, L. Mai, *Nano. Lett.* 18 (2018) 1758–1763.
- [25] N. Nakayama, T. Nozawa, Y. Iriyama, T. Abe, Z. Ogumi, K. Kikuchi, *J. Power Sources* 174 (2007) 695–700.
- [26] M. Yan, P. He, Y. Chen, S. Wang, Q. Wei, K. Zhao, X. Xu, Q. An, Y. Shuang, Y. Shao, *Adv. Mater.* 30 (2018) 1703725.
- [27] J. Zheng, Y. Hou, Y. Duan, X. Song, Y. Wei, T. Liu, J. Hu, H. Guo, Z. Zhuo, L. Liu, *Nano Lett.* 15 (2015) 6102–6109.
- [28] M. Kar, B. Winther-Jensen, M. Forsyth, D.R. MacFarlane, *Phys. Chem. Chem. Phys.* 15 (2013) 7191–7197.
- [29] F. Wang, O. Borodin, T. Gao, X. Fan, W. Sun, F. Han, A. Faraone, J.A. Dura, K. Xu, C. Wang, *Nat. Mater.* 17 (2018) 543–547.
- [30] T.K. Hoang, K.E.K. Sun, P. Chen, *RSC Adv.* 5 (2015) 41677–41691.
- [31] T. Otani, M. Nagata, Y. Fukunaka, T. Homma, *Electrochim. Acta* 206 (2016) 366–373.
- [32] K.-D. Song, K.-B. Kim, S.-H. Han, H. Lee, *Electrochem. Solid-State Lett.* 7 (2004) C20–C24.
- [33] M. Deyab, *J. Power Sources* 280 (2015) 190–194.
- [34] M. Mouanga, P. Berçot, *Corros. Sci.* 52 (2010) 3993–4000.
- [35] M. Mouanga, P. Berçot, J. Rauch, *Corros. Sci.* 52 (2010) 3984–3992.
- [36] S.J. Banik, R. Akolkar, *Electrochim. Acta* 179 (2015) 475–481.
- [37] A.S. Kannan, S. Muralidharan, K. Sarangapani, V. Balaramachandran, V. Kapali, *J. Power Sources* 57 (1995) 93–98.
- [38] K.E. Sun, T.K. Hoang, T.N.L. Doan, Y. Yu, P. Chen, *Chem.-Eur. J.* 24 (2018) 1667–1673.
- [39] K.E. Sun, T.K. Hoang, T.N.L. Doan, Y. Yu, X. Zhu, Y. Tian, P. Chen, *ACS Appl. Mater. Inter.* 9 (2017) 29681–29687.
- [40] M. Yano, S. Fujitani, K. Nishio, Y. Akai, M. Kurimura, *J. Power Sources* 74 (1998) 129–134.
- [41] O.S. Hammond, D.T. Bowron, K.J. Edler, *Angew. Chem. Int. Ed.* 56 (2017) 9782–9785.
- [42] Q. Zhang, K.D.O. Vigier, S. Royer, F. Jérôme, *Chem. Soc. Rev.* 41 (2012) 7108–7146.
- [43] A.P. Abbott, J.C. Barron, K.S. Ryder, D. Wilson, *Chem.-Eur. J.* 13 (2007) 6495–6501.
- [44] A.P. Abbott, G. Capper, K.J. McKenzie, K.S. Ryder, *J. Electroanal. Chem.* 599 (2007) 288–294.
- [45] E.S. Ferreira, C. Pereira, A. Silva, *J. Electroanal. Chem.* 707 (2013) 52–58.
- [46] C. Zhang, Y. Ding, L. Zhang, X. Wang, Y. Zhao, X. Zhang, G. Yu, *Angew. Chem. Int. Ed.* 56 (2017) 7454–7459.
- [47] A.P. Abbott, G. Capper, K.J. McKenzie, A. Glidle, K.S. Ryder, *Phys. Chem. Chem. Phys.* 8 (2006) 4214–4221.
- [48] A.P. Abbott, G. Capper, K.J. McKenzie, K.S. Ryder, *Electrochim. Acta* 51 (2006) 4420–4425.
- [49] C.R. Ashworth, R.P. Matthews, T. Welton, P.A. Hunt, *Phys. Chem. Chem. Phys.* 18 (2016) 18145–18160.
- [50] D. Shah, F.S. Mjalli, *Phys. Chem. Chem. Phys.* 16 (2014) 23900–23907.
- [51] E.L. Smith, A.P. Abbott, K.S. Ryder, *Chem. Rev.* 114 (2014) 11060–11082.
- [52] T. Zhekenov, N. Toksanbayev, Z. Kazakbayeva, D. Shah, F.S. Mjalli, *Fluid Phase Equilib.* 441 (2017) 43–48.
- [53] W.A. Henderson, F. McKenna, M.A. Khan, N.R. Brooks, V.G. Young Jr, R. Frech, *Chem. Mater.* 17 (2005) 2284–2289.
- [54] Y. Yamada, K. Usui, K. Sodeyama, S. Ko, Y. Tateyama, A. Yamada, *Nat. Energy* 1 (2016) 16129.
- [55] H. Niedermeyer, J.P. Hallett, L.J. Villar-Garcia, P.A. Hunt, T. Welton, *Chem. Soc. Rev.* 41 (2012) 7780–7802.
- [56] H. Passos, D.J. Tavares, A.M. Ferreira, M.G. Freire, Jo.A. Coutinho, *ACS Sustain. Chem. Eng.* 4 (2016) 2881–2886.
- [57] W. Shin, J. Lee, Y. Kim, H. Steinfink, A. Heller, *J. Am. Chem. Soc.* 127 (2005) 14590–14591.
- [58] A. Smith, J.C. Burns, X. Zhao, D. Xiong, J. Dahn, *J. Electrochem. Soc.* 158 (2011) A447–A452.
- [59] L. Cammarata, S. Kazarian, P. Salter, T. Welton, *Phys. Chem. Chem. Phys.* 3 (2001) 5192–5200.
- [60] M. Xu, D. Ivey, W. Qu, Z. Xie, E. Dy, X. Yuan, *J. Electrochem. Soc.* 161 (2014) A1788–A1826.
- [61] M.R. Lukatskaya, J.I. Feldblyum, D.G. Mackanic, F. Lissel, D.L. Michels, Y. Cui, Z. Bao, *Energy Environ. Sci.* 11 (2018) 2876–2883.
- [62] B. Dilasari, Y. Jung, K. Kwon, *J. Ind. Eng. Chem.* 45 (2017) 375–379.
- [63] Z. Liu, S.Z. El Abedin, F. Endres, *Electrochim. Acta* 89 (2013) 635–643.
- [64] T. Simons, A. Torriero, P. Howlett, D. MacFarlane, M. Forsyth, *Electrochem. Commun.* 18 (2012) 119–122.
- [65] M. Xu, D. Ivey, W. Qu, Z. Xie, *J. Power Sources* 252 (2014) 327–332.
- [66] H. Kim, J. Hong, K.-Y. Park, H. Kim, S.-W. Kim, K. Kang, *Chem. Rev.* 114 (2014) 11788–11827.
- [67] X. Wu, Y. Li, C. Li, Z. He, Y. Xiang, L. Xiong, D. Chen, Y. Yu, K. Sun, Z. He, *J. Power Sources* 300 (2015) 453–459.
- [68] L. Suo, O. Borodin, T. Gao, M. Olguin, J. Ho, X. Fan, C. Luo, C. Wang, K. Xu, *Science* 350 (2015) 938–943.
- [69] I. Hadjipaschalis, A. Poullikkas, V. Efthimiou, *Renew. Sustain. Energy Rev.* 13 (2009) 1513–1522.
- [70] M.R. Palacín, A. de Guibert, *Science* 351 (2016) 574.



Jingwen Zhao received his Ph.D. degree in chemistry from Beijing University of Chemical Technology in 2015. In 2014, he worked as a student visitor in University of Oxford for working on energy storage systems based on organic-inorganic hybridization. In Jul. 2015, he joined Qingdao Institute of Bioenergy and Bioprocess Technology, CAS as a faculty member. His research topics include low-cost multivalent batteries and solid-state electrolytes.



Huayu Qiu is a M.S. candidate in of Organic chemistry at Qingdao University of Science & Technology and joint training with Qingdao Institute of Bioenergy and Bioprocess Technology, Chinese Academy of Sciences. He received his B.S. degree from the Qingdao University of Science and Technology in 2017. His current research mainly engaged in secondary battery organic-inorganic hybrid electrolyte and low-cost electrochemical energy storage devices.



Jian Zhang received his M.S. degree in Chemical Engineering in 2018 from Qingdao University, and studied in Prof. Guanglei Cui's research group at the Qingdao Institute of Bioenergy and Bioprocess Technology from 2017. His research interests focus on the design of rechargeable Zn batteries and flexible electronic devices.



Shanmu Dong obtained his Ph.D. degree at the Qingdao Institute of Bioenergy and Bioprocess Technology, Chinese Academy of Sciences, in 2012. After that he worked in Qingdao Institute of Bioenergy and Bioprocess Technology, Chinese Academy of Sciences on highly efficient energy-storage materials. During 2014–2015 he came to the University of Oxford as a visiting scholar. His current research focuses on Li metal batteries.



Wuhai Yang is pursuing his M.S. degree in Qingdao University of Science & Technology majoring in polymer chemistry and physics. He received his B.S. degree from the Qingdao University of Science and Technology in 2017. His current research focuses on the design of electrolytes for multivalent secondary batteries.



Xinhong Zhou received her Ph.D. in 2005 from the department of Chemistry, Tsinghua University. She became associate professor at the College of Chemistry and Molecular Engineering at Qingdao University of Science & Technology in 2010. Her research interests focus on the design and synthesis of new materials in high-energy density secondary batteries.



Bingbing Chen received his Ph.D. degree in 2016 from the Nanjing Tech University. He is currently a postdoctoral researcher in Materials Science and Engineering at the Qingdao Institute of Bioenergy and Bioprocess Technology, Chinese Academy of Sciences. His work focuses on all-solid-state lithium batteries with a high energy density and the stability of the electrode/electrolyte interface.



Guanglei Cui received his Ph.D. from ICCAS (2005). From 2005–2009, he had worked at Max-Planck-Institute for Polymer Research and Solid State research as a postdoctoral scientist on Ener. Chem. Project. Then he joined in the QIBEBT as professor from 2009. His research interests include low-cost and highly efficient energy-storage materials, electrode materials, and novel energy devices including lithium ion batteries, super-capacitors, and perovskite solar cells.



Zhiming Zhao got his Bachelor's degree from Northeast Forestry University in 2016. Currently he is a PhD student under the supervision of Prof. Guanglei Cui at Qingdao Institute of Bioenergy and Bioprocess Technology, Chinese Academy of Sciences. His work involves structure design and protection for anodes of new-type batteries.



Liquan Chen is a professor in Institute of Physics, Chinese academy of Science. He is an academican of Chinese Academy of Engineering. In China, he has initiated the researches on lithium super ionic conductor and solid lithium batteries since 1982, first principle calculation in batteries in 2001 and earliest pilot production of 18,650 line. His current research interests include advanced materials, devices and related fundamental researches in high energy density lithium ion batteries, solid lithium batteries and high-throughput efforts in solid batteries.